

Self-supervised machine learning model for analysis of nanowire morphologies from transmission electron microscopy images

Shizhao Lu¹, Brian Montz², Todd Emrick², Arthi Jayaraman^{1,3*}

¹Department of Chemical and Biomolecular Engineering, University of Delaware, 150 Academy St., Newark, DE 19716, United States

²Department of Polymer Science and Engineering Department, University of Massachusetts Amherst, Amherst, Massachusetts 01003, United States

³Department of Materials Science and Engineering, University of Delaware, 201 DuPont Hall, Newark, DE 19716, United States

Correspondence to: arthij@udel.edu

Abstract:

In the field of soft materials, microscopy is the first and often only accessible method for structural characterization. There is a growing interest in the development of machine learning methods that can automate the analysis and interpretation of microscopy images. Typically training of machine learning models require large numbers of images with associated structural labels, however, manual labeling of images requires domain knowledge and is prone to human error and subjectivity. To overcome these limitations, we present a self-supervised transfer learning approach that uses a small number of labeled microscopy images for training and performs as effectively as methods trained on significantly larger data sets. Specifically, we train an image encoder with unlabeled images and use that encoder for transfer learning of different downstream image tasks (classification and segmentation) with a minimal number of labeled images for training.

1. Introduction

Within the broad field of soft materials where structure often drives function, structural characterization is a key step in the discovery of novel functional materials.^{1,2} For most researchers, microscopy imaging is the first and, in many cases, only accessible means to obtain structural information. Depending on the length scale of interest, commonly used techniques include optical microscopy, transmission electron microscopy (TEM), scanning electron microscopy (SEM), and atomic force microscopy (AFM). Regardless of the technique, each microscopy image is associated with the chemical composition of the material, region/section of the material that is imaged, and the processing conditions for the imaging. The resulting images may resemble a heat map of intensity highlighting object(s) owing to the selective staining of some species/sections in the sample.³ Analyzing these microscopy images requires domain knowledge to interpret (e.g., classify images with morphology labels) and/or to detect nuances in different images (e.g., identification of defects, changes in intensity, etc.) as the composition or the focus of the image or the processing condition is changed. Thus, manual interpretation is often time-consuming, labor-intensive, and prone to human subjectivity in interpretation. Therefore, machine learning (ML) has become a valuable tool that can replace time-consuming and subjective manual interpretation of microscopy image with automated, objective, and fast analysis.^{4,5}

Development of traditional ML models relies heavily on the procurement of big datasets related to a specific task. To bypass the need to collect large training data and reduce the time needed to train the ML model from scratch on that large data, researchers use ‘transfer learning’ (TL) techniques.⁶ TL involves leveraging the knowledge of a model previously trained using large training datasets to create a new model for another related task. For example, a model that has been trained on ImageNet⁷, a large dataset of 1.2 million photographic images of macroscopic objects,

can be transferred to learn how to analyze images in another more specific domain [e.g., medical image classification ⁸ or morphology classification of soft materials ⁹]. The success of TL in the field of image analysis has paved the way for accessibility to pretrained image learning models for the general public without requiring large computational resources or big data to train from scratch.

10

TL for microscopy image analysis tasks has traditionally relied on convolutional neural network (CNN) models ¹¹ which convert input images into feature maps that hold information for image classification (e.g., assigning a morphology label to a microscopy image) and detection of objects in the image (e.g., identification of a nanoparticle aggregate or domain). In TL, the weights of some layers of the pre-trained CNN are kept as constants and only the weights for the outermost layer are retrained with images for the specific task at hand. In most implementations of TL, the microscopy image dataset for the specific task has to be labeled (i.e., supervised learning) before training the outermost layer. However, CNN models trained on one type of supervised tasks (classification, segmentation, or object detection) can typically only be transferred to the same supervised task for another image dataset which limits the generalized applicability of TL. Further, the typical size of image datasets needed for training ranges from thousands to hundreds of thousands of images, even with transferred models, and the labeling of these large set of images is challenging and prone to error, with a recent study noting (on average) 3.3% labeling errors in large open source datasets. ¹²

To overcome limitations of labeling, self-supervised learning of images has emerged as a new form of label-free training. ¹³ Through self-supervised training, the ML model learns a representation of an image by maximizing the similarity between two different transformed versions of the same image. While supervised model training is assisted by the labels associated

with each image, self-supervised model training does not rely on labels and learns from the underlying features of the images. The performance of self-supervised TL has been shown to be comparable with supervised TL in big data medical image classification.^{14,15} For example, Azizi et al. have achieved 70% classification accuracy on dermatology images (using ~450,000 images for training) with self-supervised TL¹⁴ and Ciga et al. have achieved 78% classification accuracy on a diverse set of histopathology images (using ~40,000 images for training) with self-supervised TL.¹⁵ In contrast to the medical imaging field which traditionally has large data sets, researchers in the soft materials domain handle much smaller datasets and have a more diverse range of image analysis tasks. Thus, for self-supervised TL to be accessible to researchers in soft materials, it has to be adapted to small dataset sizes and be able to handle multiple tasks (e.g., classification and segmentation). In this report, we present an automated, label-efficient ML workflow that can identify the type of structure and outline objects in microscopy images with high accuracy after training on only a handful of carefully labeled microscopy images.

We focus on a self-supervised TL workflow to perform automated classification and segmentation of TEM images taken from one class of soft materials – protein and peptide nanowires – which are used in a wide variety of applications including flexible electronics¹⁶, energy harvest¹⁷, and chemical sensing¹⁸. In all these applications, the nanowire morphologies (e.g., dispersed, aggregated, percolated, phase separated) dictate their performance. In this work, we use TEM images from assembled, synthetically engineered, peptide nanowires and biologically derived (from *Geobacter sulfurreducens*) protein nanowires¹⁹ to demonstrate a self-supervised TL workflow that shows high accuracy in classification and segmentation of these images with <1000 generic unlabeled training images and <10 task-specific images with labels per morphology class.

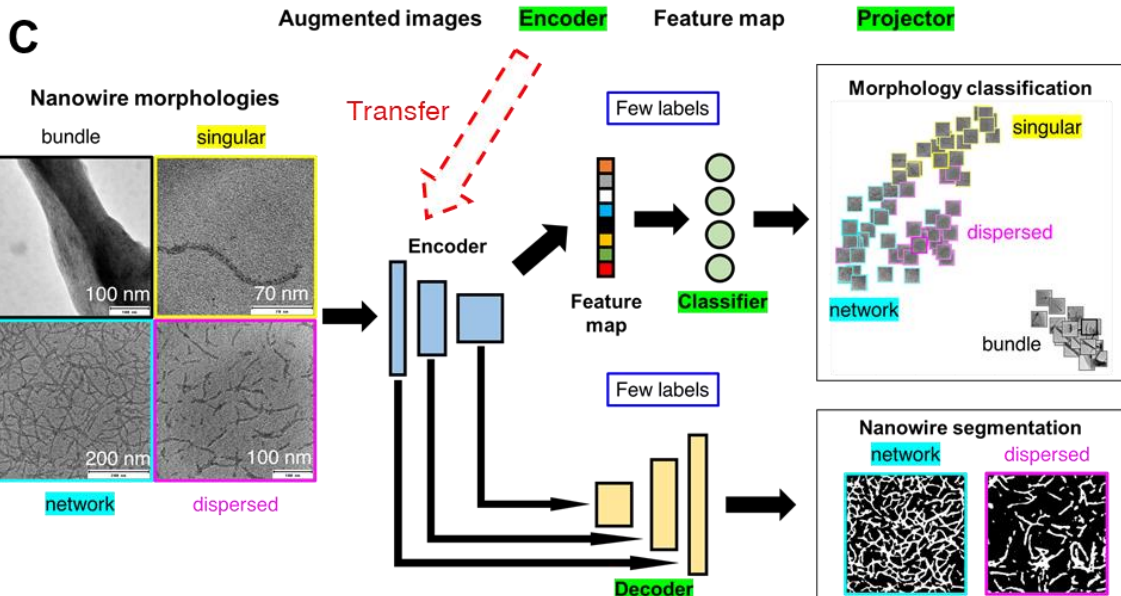
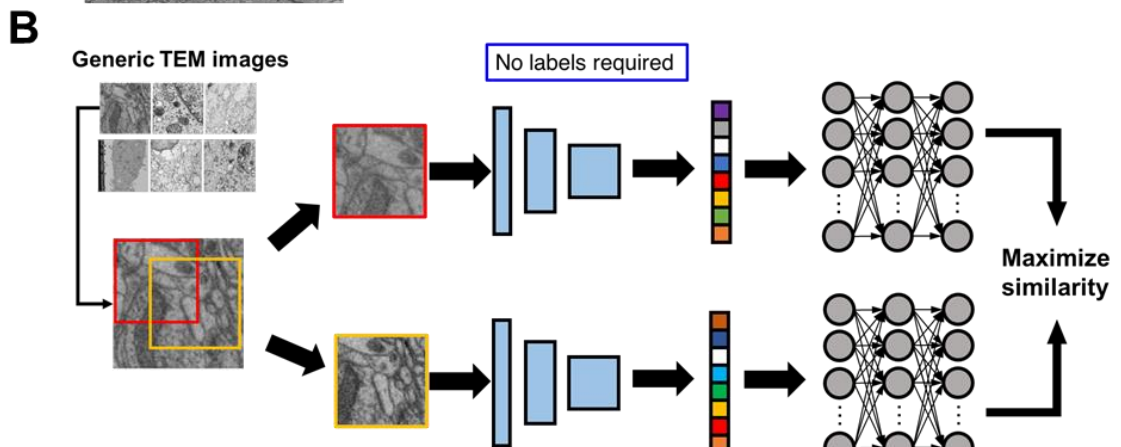
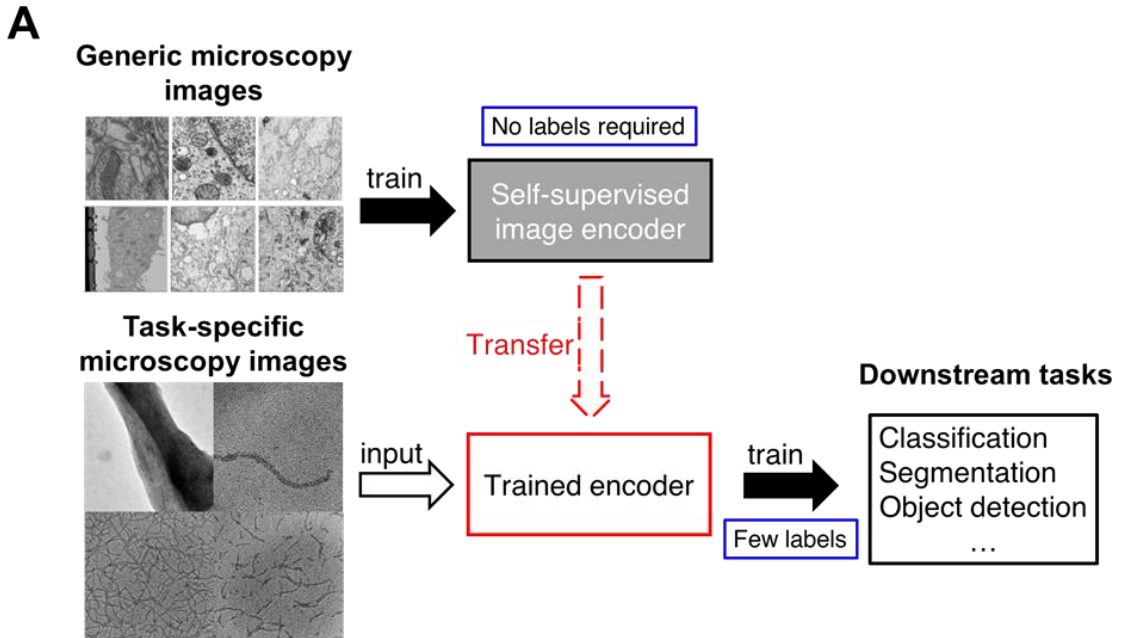


Fig. 1. Machine learning workflow for classification and segmentation of microscopy images.

(A) Two-step generalized self-supervised workflow for microscopy image learning. An image encoder is first trained on generic microscopy images ²⁰ (permission from eLife Sciences Publications, Ltd, UK under [CC-BY license](#)) without supervision, i.e., self-supervised. Then, the *self-supervised image encoder* is transferred to convert task-specific microscopy images into feature maps which are used to train multiple models for downstream tasks (e.g., classification, segmentation) **(B)** For each image in the generic TEM image dataset, two randomly augmented images are generated. To maximize the similarity between the two augmented images, an encoder (ResNet50 ²¹), followed by a projector made of three fully connected neural layers, are trained. **(C)** The encoder is transferred as is for the task-specific image encoding (i.e., to convert TEM images of nanowire morphologies to feature maps) followed by supervised, label-efficient training of classifier and decoder for downstream tasks – classification and segmentation of TEM images.

2. Results and discussions

We illustrate the conceptual workflow of self-supervised transfer learning for microscopy images in **Fig. 1A**. First, a generic image learning model, an encoder, undergoes self-supervised training (i.e., no labels required during training) on a dataset of generic microscopy images ²⁰. We transfer the trained encoder to transform images into feature maps (i.e., vectorized representations of images) for training of downstream tasks. We demonstrate the self-supervised workflow with a detailed example of TL of nanowire morphologies from generic TEM images. We start by training the encoder with self-supervised methods on generic TEM images (**Fig. 1B**). We implement two self-supervised training methods: SimCLR ¹³ and Barlow-Twins ²². Both methods start by taking a batch of images and generating two randomly augmented images for each image by performing

random color/hue/contrast changes, and/or randomly crop a portion of the image. The augmented images are then turned into feature maps by an encoder with ResNet50²¹ architecture. The feature maps are input into a projector with three layers of fully connected neurons to generate projections of each image. The projections are then used to calculate and minimize the loss function to train both the encoder and the projector. Through maximizing the similarity between two augmented images of the same image, the encoder is trained to produce feature maps that can represent the images more accurately. The difference between the two methods – SimCLR¹³ and Barlow-Twins²² – is in the loss function as described in the methods section. The trained encoder is then transferred to learn the protein/peptide nanowire morphologies (**Fig. 1C**). For the classification task, we use the simplest linear classifier consisting of four neurons equivalent to the number of morphology classes to classify the feature maps. For the image segmentation task, we use U-Net²³, an established deep learning architecture that has been shown to outperform traditional segmentation methods^{24,25}. The original U-Net architecture consists of an encoder and a decoder trained to create accurate segmentation of input images. Instead of the original U-Net architecture, we use our trained encoder with trained weights to establish skip connections between our encoder and a decoder with random initialized weights (**Fig. S1**).

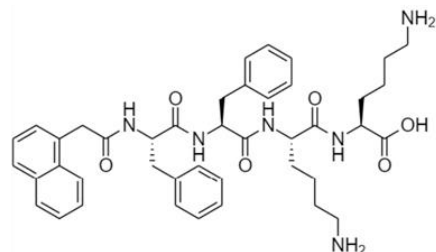
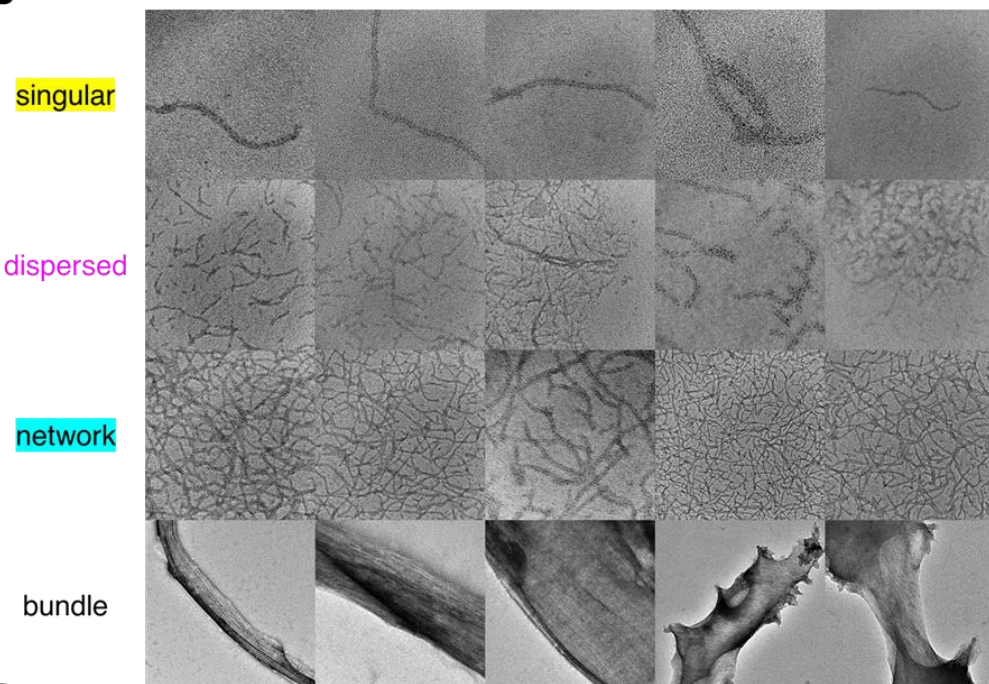
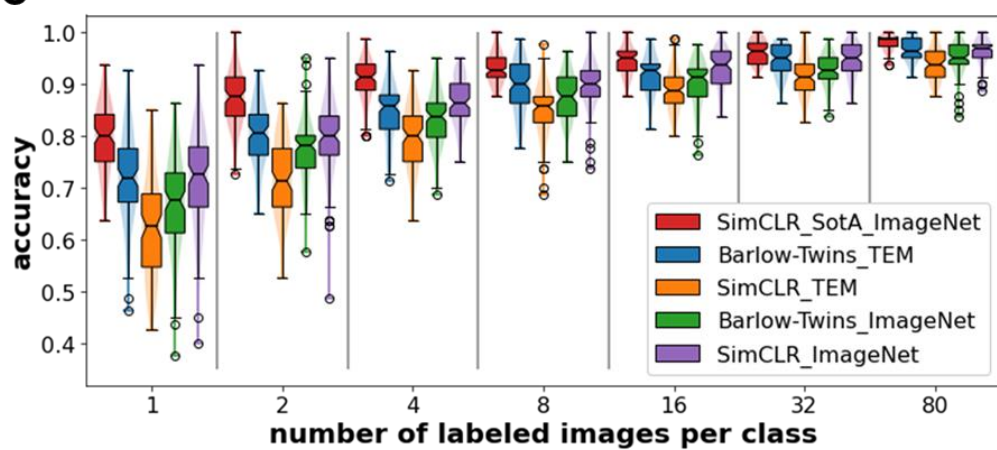
A**B****C**

Fig. 2. Nanowire chemical composition, TEM images of nanowire morphologies, and performance of the trained model for classification task. (A) N-[2-(1-Naphthalenyl)acetyl]-L-phenylalanyl-L-phenylalanyl-L-lysyl-L-lysine (NapFFKK) oligopeptide structure that self-

assembles into singular, dispersed, and network nanowire morphologies from water and organic solvents. **(B)** Representative TEM images of the four types of nanowire morphologies labeled in the figure; apart from the three oligopeptide nanowire morphologies, the bundle morphology is obtained from pilA protein nanowires (amino acid sequence of pilA: FTLIELLIVVAAIGILAAIAIPQFSAYRVKAYNSAASSDLRNLKTALESAFADDQTYPPES) harvested biologically from *Geobacter sulfurreducens* and assembled in organic solvents. **(C)** Classification accuracy of the trained model as a function of number of labeled images used during training. Legend denotes the self-supervised method and the generic image dataset used to train the encoder. Sample size is 100 for each boxplot. Notch of the boxplots indicates 95% confidence interval around the median.

Protein / peptide nanowires exhibit one of four morphologies when dispersed in solvent – singular (i.e., isolated nanowire), dispersed (i.e., isolated collection of multiple nanowires), network (i.e., percolated nanowires), and bundle morphologies. Materials with dispersed nanowires are desired for mechanical reinforcement ²⁶, while materials with network morphologies are desired for improving conductivity ¹⁶. The singular, dispersed, and network morphologies in this work arise from assembly of synthetic oligopeptides shown in **Fig. 2A**; the bundle morphologies represent aggregates of protein nanowires harvested from *Geobacter sulfurreducens*. 100 images from each morphology are employed (**Fig. 2B**). As the dispersed and network morphologies are harder to visually distinguish, we manually label the nanowires in the images through Microscopy Image Browser (MIB) ²⁷. This manual labeling serves two purposes: 1) to provide pixel-level quantification of percolation (in network) or lack thereof (in dispersed) and 2) to provide ground truth labels of nanowires for the segmentation task. A percolation analysis of the clusters of manually labeled nanowires distinguishes the networks (percolated) and dispersed (not percolated)

nanowire morphologies. Except for the state-of-the-art (SotA) encoder which we obtained as a published open-access encoder trained with SimCLR method on the full ImageNet dataset (1.26 million images), other models are trained with optimized hyperparameters (**Fig. S2**). The Barlow-Twins method is insensitive to various hyperparameters and enables training of higher resolution images as input without compromise in classification accuracy (**Fig. S3**). To show whether transferring learned weights from a domain-specific dataset gives better model performance, we trained the two self-supervised encoders on 832 generic TEM images or 832 generic everyday photographic images from ImageNet, both at resolution 224×224 . We report the classification accuracies from the linear classifier on the feature maps of the test sets (**Fig. 2C**). When trained with generic TEM images, the Barlow-Twins method outperforms SimCLR method. When trained with Barlow-Twins method, transferring from domain-specific images, i.e., TEM images, brings higher performance than transferring from everyday images. However, when trained with SimCLR method, transferring from domain-specific images underperforms transferring from images of other domains. We believe that SimCLR performs worse when trained on generic TEM images due to the reduced contrast in generic TEM images compared to that in ImageNet images. Strikingly, feature maps obtained from the Barlow-Twins-TEM encoder obtain $>90\%$ classification accuracy when trained with just 8 labeled images per class. With more numbers of labeled images, feature maps obtained from the Barlow-Twins-TEM encoder achieve comparable classification accuracy to that of feature maps obtained from the SotA encoder. We show that prediction from feature maps extracted using self-supervised trained encoders give high accuracy when only trained with few labeled images.

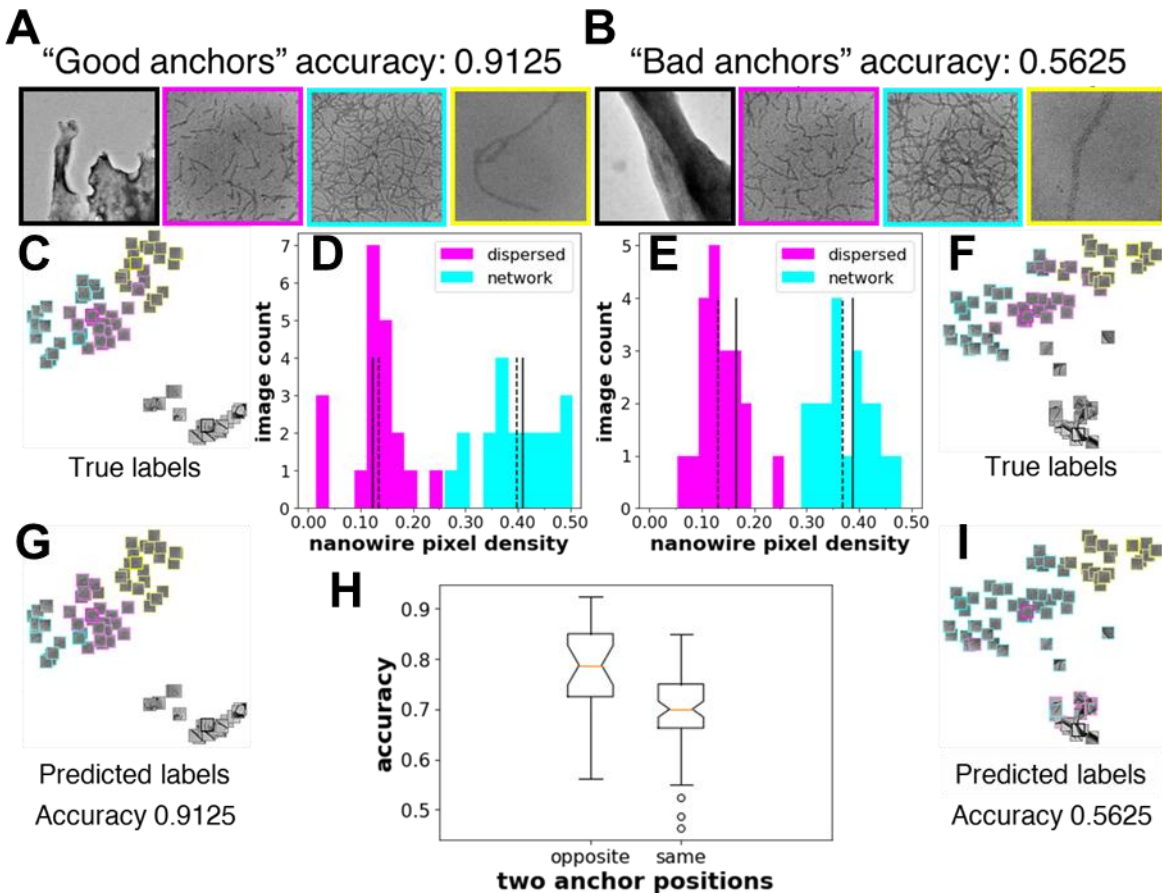


Fig. 3. Knowledge of the underlying distribution of the images can help determine good “anchor” images for high accuracy one-shot learning. (A and B) Good “anchor” images i.e., a set of labeled images from each morphology, which when used for training give high classification accuracy. Bad “anchor” images which when used for training give low classification accuracy. t-SNE²⁸ representations of the test set colored by their true labels and by their predicted labels with “good anchor” images as training set (**C, G**) and “bad anchor” images as training sets (**F, I**). The image count distribution with nanowire pixel density obtained from the manual nanowire labels for the dispersed and network morphology images in the test set with “good anchors” (**D**) and “bad anchors” (**E**) images as training sets, respectively. Solid lines are positions of the two “anchors”, and dashed lines are positions of the two medians. Test set size is 20 for both dispersed and network

morphology. **(H)** The positions of the two “anchors” relative to the median of the dispersed and network images in the test set. For the 100 samples obtained in Fig. 2C for Barlow-Twins-TEM, 25 resulted on the opposite side, 75 resulted on the same side. Notch of the boxplots indicates 95% confidence interval around the median.

As we observe large fluctuations in the accuracy of linear classifiers trained with only one labeled image per class (i.e., one-shot learning), we want to understand how to select the labeled images or the “anchor” images for high accuracy. Using feature maps obtained from the Barlow-Twins-TEM encoder, we show one example of “good anchors” and “bad anchors” each chosen posteriorly from the accuracies (**Fig. 3A-3B**). We use t-distributed Stochastic Neighbor Embedding (t-SNE)²⁸ to visualize the feature maps of the test images projected in 2-dimensional space. From the t-SNE plots, we see that while there are few misclassifications between the dispersed and network morphologies when the linear classifier is trained on “good anchors” (**Fig. 3C and 3G**), most images in dispersed morphology are misclassified as network morphology when the linear classifier is trained on “bad anchors” (**Fig. 3F and 3I**). To explain the visible difference in the performance of linear classifiers trained on different “anchors”, we look at the distribution of the nanowire pixel density, i.e., percentage of “nanowire pixels” over all pixels, of the ground truth (i.e., manually labeled images with nanowire pixels and background pixels) for test images in dispersed and network morphologies. The nanowire pixel density of the two anchor images is on the opposite sides of that of the respective median of the two morphologies for “good anchors” (**Fig. 3D**), but on the same sides for “bad anchors” (**Fig. 3E**). We also show the statistics of all 100 sets of anchors and find that the accuracy of linear classifiers trained on “opposite side anchors” is statistically higher than that trained on “same side anchors” (**Fig. 3H**). We conclude that

“opposite side anchors” are good approximates of the medians thereby leading to good accuracy, but “same side anchors” are not.

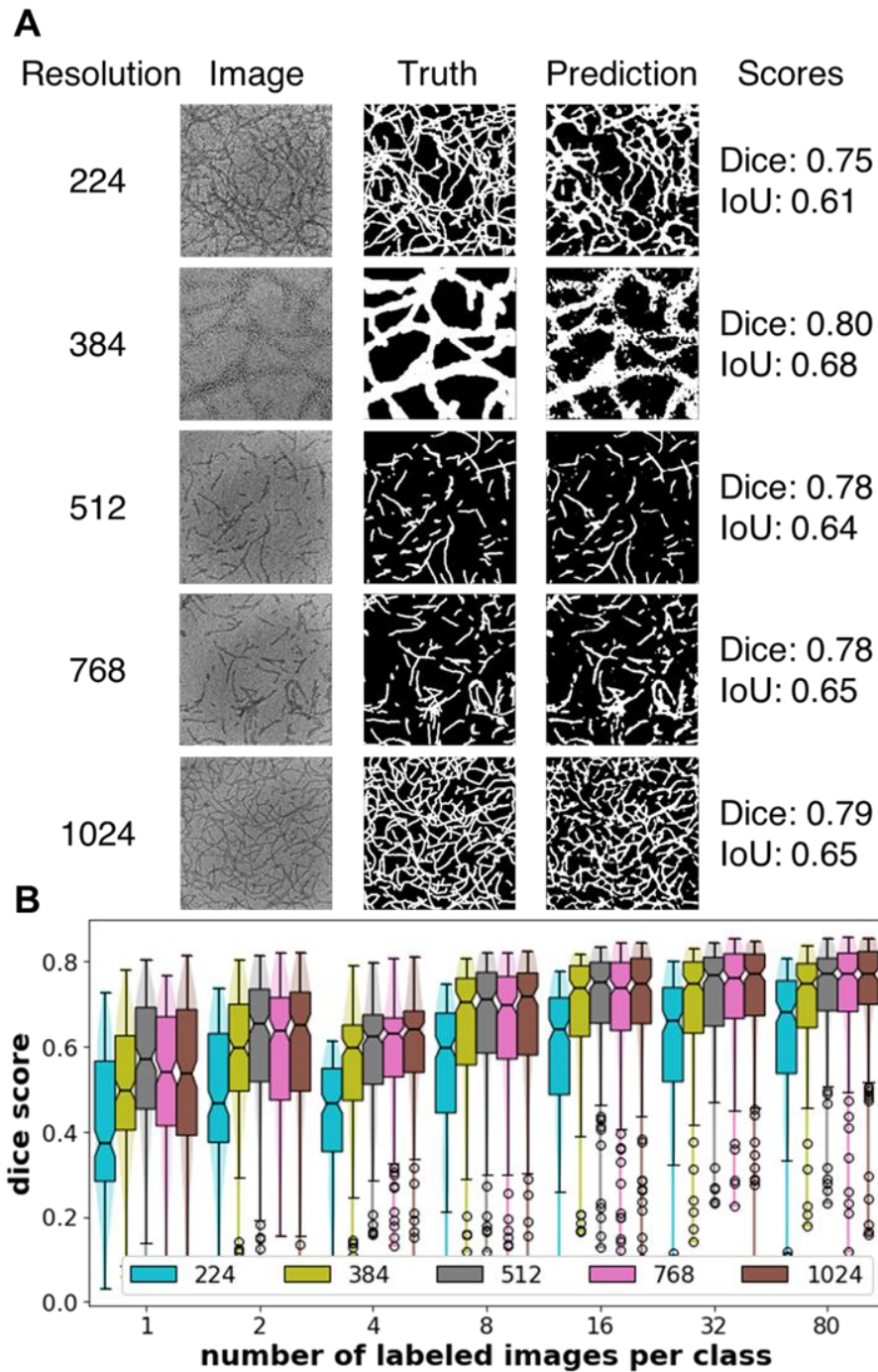


Fig. 4. Nanowire segmentation task performance. (A) Original image, manually labeled nanowires, predicted nanowires, and segmentation performance dice scores and intersection-over-union (IoU) scores at five input image resolutions. (B) Dice scores for the nanowire segmentation task. Legend indicates the resolution of the input images. Sample size is 200 for each boxplot. Notch of the boxplots indicates 95% confidence interval around the median.

Next, we tackle the task of segmentation of nanowires for the dispersed and percolated morphologies. We calculate both the dice score (Eq. S1) and the Intersection-over-Union (IoU) score (Eq. S2) for each prediction. Our U-Net model with transferred encoder (trained on resolution of 512×512 unlabeled generic TEM images with the Barlow-Twins method) works well with images of resolutions up to 1024×1024 (Fig. 4A). Of the five input resolutions, our U-Net model trained with images of resolution 224 underperforms the higher resolution images likely due to poor contrast when the images are resized to such low resolution. We observe a plateau in the dice score from 8 to 80 labeled images per class and a drop-off from having 8 down to 4 labeled images per class (Fig. 4B). With transferred encoder, our Unet model can achieve good performance with just 8 labeled images per class for training, less than half of the number of test images (20 per class). IoU scores follow the same qualitative trend as dice scores; the values of IoU scores are always smaller than dice scores (Fig. S4). Encoder trained with unlabeled images of different resolutions give statistically similar dice and IoU scores (Figs. S5 and S6).

3. Summary and conclusion

In summary, we have demonstrated the efficacy of a self-supervised transfer learning workflow applied to the task of learning nanowire morphologies from a small dataset and minimum number

of manual labels. We show that our encoder trained with <1000 unlabeled images achieve comparable performance with state-of-the-art encoder trained with more than one million images. Self-supervised transfer learning workflow can be applied to other soft material domains of microscopy images learning with limited available images for training. Our downstream task models trained on the encoded feature maps can achieve $>90\%$ accuracy on classification of nanowire morphologies training with <10 labeled images per class. With knowledge of the underlying image distribution of the two morphologies that are harder to visually distinguish, we show that it is possible to achieve $>90\%$ accuracy training with just one labeled image per morphology. Our trained encoders can aid in microscopy imaging of soft materials in automatic feature extraction and further image classification, and regression, requiring minimal labeled training data.

REFERENCES

- 1 Cubuk, E. D. *et al.* Structure-property relationships from universal signatures of plasticity in disordered solids. *Science* **358**, 1033-1037 (2017).
- 2 Huang, C., Chen, X., Xue, Z. & Wang, T. Effect of structure: A new insight into nanoparticle assemblies from inanimate to animate. *Science advances* **6**, eaba1321 (2020).

3 Goodhew, P. J., Humphreys, J. & Beanland, R. *Electron microscopy and analysis*. (CRC press, 2000).

4 Ge, M., Su, F., Zhao, Z. & Su, D. Deep learning analysis on microscopic imaging in materials science. *Materials Today Nano* **11**, doi:10.1016/j.mtnano.2020.100087 (2020).

5 Baskaran, A. *et al.* Adoption of Image-Driven Machine Learning for Microstructure Characterization and Materials Design: A Perspective. *JOM* **73**, 3639-3657 (2021).

6 Yosinski, J., Clune, J., Bengio, Y. & Lipson, H. How transferable are features in deep neural networks? *Advances in neural information processing systems* **27** (2014).

7 Krizhevsky, A., Sutskever, I. & Hinton, G. E. ImageNet classification with deep convolutional neural networks. *Commun. ACM* **60**, 84–90, doi:10.1145/3065386 (2017).

8 Kermany, D. S. *et al.* Identifying medical diagnoses and treatable diseases by image-based deep learning. *Cell* **172**, 1122-1131. e1129 (2018).

9 Luo, Q., Holm, E. A. & Wang, C. A transfer learning approach for improved classification of carbon nanomaterials from TEM images. *Nanoscale Advances* **3**, 206-213 (2021).

10 von Chamier, L. *et al.* Democratising deep learning for microscopy with ZeroCostDL4Mic. *Nature communications* **12**, 1-18 (2021).

11 LeCun, Y., Bengio, Y. & Hinton, G. Deep learning. *Nature* **521**, 436-444 (2015).

12 Northcutt, C. G., Athalye, A. & Mueller, J. Pervasive label errors in test sets destabilize machine learning benchmarks. *arXiv preprint arXiv:2103.14749* (2021).

13 Chen, T., Kornblith, S., Norouzi, M. & Hinton, G. in *International conference on machine learning*. 1597-1607 (PMLR).

14 Azizi, S. *et al.* in *Proceedings of the IEEE/CVF International Conference on Computer Vision*. 3478-3488.

15 Ciga, O., Xu, T. & Martel, A. L. Self supervised contrastive learning for digital histopathology. *Machine Learning with Applications* **7**, 100198 (2022).

16 Sun, Y. L. *et al.* Conductive Composite Materials Fabricated from Microbially Produced Protein Nanowires. *Small* **14**, 1-5, doi:10.1002/smll.201802624 (2018).

17 Liu, X. *et al.* Power generation from ambient humidity using protein nanowires. *Nature* **578**, 550-554, doi:10.1038/s41586-020-2010-9 (2020).

18 Smith, A. F. *et al.* Bioelectronic protein nanowire sensors for ammonia detection. *Nano Research*, 1-6 (2020).

19 Reguera, G. *et al.* Extracellular electron transfer via microbial nanowires. *Nature* **435**, 1098-1101 (2005).

20 Conrad, R. & Narayan, K. CEM500K, a large-scale heterogeneous unlabeled cellular electron microscopy image dataset for deep learning. *Elife* **10**, e65894 (2021).

21 He, K., Zhang, X., Ren, S. & Sun, J. in *Proceedings of the IEEE conference on computer vision and pattern recognition*. 770-778.

22 Zbontar, J., Jing, L., Misra, I., LeCun, Y. & Deny, S. in *International Conference on Machine Learning*. 12310-12320 (PMLR).

23 Ronneberger, O., Fischer, P. & Brox, T. in *International Conference on Medical image computing and computer-assisted intervention*. 234-241 (Springer).

24 Yao, L., Ou, Z., Luo, B., Xu, C. & Chen, Q. Machine learning to reveal nanoparticle dynamics from liquid-phase TEM videos. *ACS central science* **6**, 1421-1430 (2020).

25 Karabağ, C., Verhoeven, J., Miller, N. R. & Reyes-Aldasoro, C. C. Texture segmentation: An objective comparison between five traditional algorithms and a deep-learning U-Net architecture. *Applied Sciences* **9**, 3900 (2019).

26 Tadiello, L. *et al.* The filler–rubber interface in styrene butadiene nanocomposites with anisotropic silica particles: morphology and dynamic properties. *Soft Matter* **11**, 4022-4033 (2015).

27 Belevich, I., Joensuu, M., Kumar, D., Vihinen, H. & Jokitalo, E. Microscopy image browser: a platform for segmentation and analysis of multidimensional datasets. *PLoS biology* **14**, e1002340 (2016).

28 Van der Maaten, L. & Hinton, G. Visualizing data using t-SNE. *Journal of machine learning research* **9** (2008).

ACKNOWLEDGMENTS

Funding: The authors acknowledge financial support from the U.S. National Science Foundation, Grant NSF DMREF #1921839 and DMREF #1921871.

Author contributions: S.L. devised the idea and led the machine learning workflow development with guidance and feedback from A.J.; B.M. performed the synthesis of the synthetic peptide nanowires and microscopy imaging for the synthetic peptide nanowires and bioderived protein nanowires with feedback from T. E.; B.M. and S.L. decided on the qualification criteria of different morphologies; S.L. created the segmentation ground truth labels and the morphology class labels; S.L. wrote the python code for implementing the model and trained the models; S.L., B.M., T. E., and A.J. wrote the manuscript.

Competing interests: The authors declare no competing interests.

Data and materials availability: The python code for implementing these models with Keras and Tensorflow is available at <https://github.com/arthijayaraman-lab/self->

supervised_learning_microscopy_images. The image dataset of nanowire morphologies is deposited on the open-access data repository Zenodo with DOI: 10.5281/zenodo.6377141.

Supplementary information is available from the corresponding author upon request.